Journal of Materials Chemistry A

Accepted Manuscript

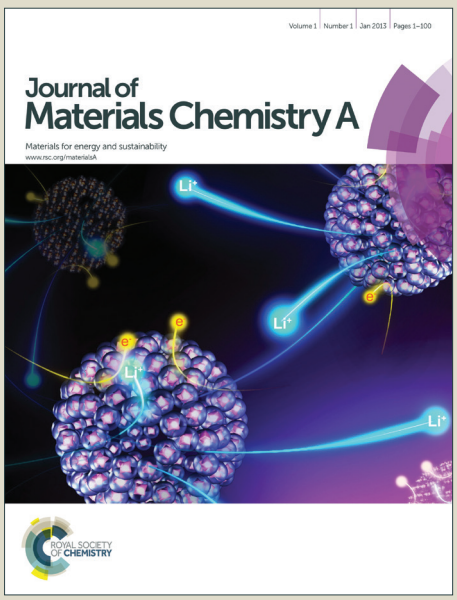

ROYAL SOCIETY OF CHEMISTRY

www.rsc.org/materialsA

Journal Name

ARTICLE

Ultra-small Sulphur Nanoparticles Configured Inside a Flexible Organic Mixed Conducting Network as Cathode for Lithium-Sulphur Battery

Sudeshna Sen[a], Dipak Dutta[a], Aninda J. Bhattacharyya[a*]

Received 00th January 20xx,
Accepted 00th January 20xx

DOI: 10.1039/x0xx00000x

www.rsc.org/

The major challenges in a Li-S battery are the formation of soluble polysulphides during the reversible conversion of $S_8 \leftrightarrow Li_2S$, large changes in sulphur particle volume during lithiation and extremely poor charge transport in sulphur. We demonstrate here a novel and simple strategy to overcome these challenges towardspractical realization of a stable high performance Li-S battery. For the first time, astrategyis developedwhich does away with the necessity of pre-fabricated high surface area hollow-structuredadsorbates and also multiple nontrivial synthesis steps related to sulphur loading insidesuch adsorbates. Lithiated polyethylene glycol (PEG) based surfactant tethered on ultra-small sulphur nanoparticles wrapped up with polyaniline (PAni) (abbreviated S-MIEC) is demonstrated here as an exceptional cathode for Li-S battery. The PEG and PAni network around the sulphur nanoparticles serve as an efficient flexible trap for the sulphur and polysulphides and also provides distinct pathways for electrons (through PAni) and ions (through PEG) during battery operation. Contrary to the cathodes demonstrated based on various carbon-sulphur composites, the mixed conducting S-MIEC showed an extremely high loading of 75%. The S-MIEC exhibited a stable capacity of nearly 900 $mAhg^{-1}$ at the end of 100 cycles at 1 C current rate.

Introduction

The rapid depletion in fossil fuel stocks coupled with drastic increase in the energy consumption have led to serious efforts towards the development of technologies and devices based on alternative sources of energy such as electrochemical energy.[1] High energy and power density rechargeable batteries have a great potential to cater to a variety of human needs. Among rechargeable battery chemistries, lithium-based batteries especially lithium-ion has shown great promise in a variety of applications ranging from mobile electronics to electrical vehicle. However, lithium-ion batteries have achieved partial success owing to limitations in energy storage primarily due to the usage of intercalation oxide cathodes (IOCs).[2,3]Despite substantial progress in the development of high capacity anodes (e.g. Si nanostructured anodes)[4]the availability of high specific capacity cathodes are scarce and still poses a formidable challenge towards development of high energy and power density lithium-ion batteries.

[a]*Solid State and Structural Chemistry Unit, Indian Institute of Science, Bangalore, 560012, India. *E-mail: aninda_jb@sscu.iisc.ernet.in*
Electronic Supplementary Information (ESI) available: [details of any supplementary information available should be included here]. See DOI: 10.1039/x0xx00000x

Usage of elemental cathodes instead of compound cathodes has been suggested to drastically improve the quantum of energy storage in rechargeable batteries. In this context sulphur is very promising due to its high theoretical capacity of 1672 $mAhg^{-1}$ (gravimetric energy density = 2500 $Whkg^{-1}$), which is an order higher than the best known IOCs.[2] Despite the advantage of high capacity of sulphur, the Li-S battery is still far from widespread practical realization. The major hurdles that come in the way of commercialization of Li-S battery are (i) the various soluble polysulphides formed during the course of the reversible conversion of $S_8 \leftrightarrow Li_2S$ and (ii) the exceptionally large volume expansion of sulphur (80%) taking place during successive cycling.[5] During the discharge process, the soluble polysulfide anion (Li_2S_x, $4 \le x \le 8$) migrate through the separator to the negative lithium anode where they are reduced and get deposited as insoluble products i.e. Li_2S_2 and/or Li_2S. This results in the passivation of the anode. Also uninterrupted reduction of Li_2S_x to Li_2S_2 and Li_2S at the anode prevents their re-oxidation to elemental sulphur at the cathode during the charging cycle. This process, known as the polysulfide "shuttle" phenomenon, gradually decreases the active mass of sulphur loading to continuous fading in capacity and limiting the performance of sulphur cathodes much below the theoretical limit of 1675 $mAhg^{-1}$.[5-11]Thus, usage of a strong adsorbate of Li_2S_x so as to minimize the loss in the active mass of the cathode has been so far suggested to be absolutely essential for a long life Li-S battery. Another detrimental factor, in addition to the above mentioned points (under (1) and (ii)), for a stable Li-S battery is related to the insulating nature of sulphur (ionic conductivity$\approx 5\times10^{-30}\Omega^{-1}cm^{-1}$ and electronic conductivity$\approx 2.0\times10^{-17}\Omega^{-1}cm^{-1}$ at 25°C).[12]This necessitates the usage of an adsorbing host which should also be conducting for operation at high current values. In this regard, several developed approaches solely target at confining sulphur inside various high surface area hollow electronically conductive carbon hosts.[12-14]The main drawback with this approach is the uncertainty in the spatial distribution of sulphur with respect to the carbon host. More often than not the precise loading of sulphur inside the carbon host is not clearly discussed and can in fact, be very low. Such uncertainties can be completely avoided and electrochemical performance can be drastically improved if the sulphur can be suitably configured inside a flexible as well as a mixed conducting environment. In this light, we demonstrate here a lithiated polyethylene glycol (PEG) based surfactant tethered on ultra-small sulphur nanoparticles wrapped up with polyaniline (PAni) (abbreviated as S-MIEC) as an exceptional cathode for Li-S battery. This approach, apart from ensuring precise distribution and location of sulphur with regard to the flexible host, has two other benefits. Firstly, the mixed conducting framework around sulphur provides efficient and distinct electron and ion transport pathways during lithiation / delithiation processes. Secondly, the space available can be used to trap the polysulphides and provide free space to accommodate the changes in sulphur volume. There have been very few reports demonstrating the concept of integration of the active storage materials with an organic mixed conducting polymer matrix.[15]In the published reports the adopted approach however, has led to a final product predominantly resembling more an additive mixture of the active material and polymer components.

Results and Discussion

Polyaniline (PAni), a well-known synthetic organic polymer which when doped with an acid (i.e. p-doped) becomes an electronic conductor. During the doping process an electron is removed from the PAni backbone producing a free radical and a spinless positive charge; the radical and the positive charge are coupled to each other via local resonance of the charge and the radical and is known as "polaron".[16] Chemically, polaron is a localized radical ion associated with lattice distortion. After the formation of polarons, on further oxidation or removal of electrons from polymer chains, result in the formation of a pair of similar charges (spinless) which are associated with strong local vibration, and are known as "bi-polaron".[16]The polaron-bipolaron charge transport result in very high electronic conductivity in PAni reaching a value of (0.18-0.31) $\Omega^{-1}cm^{-1}$ in PAni/HCl.[17]It is also known that incorporation of polyethylene glycol (PEG) into sulphur composite creates a chemical gradient in the composite that retards the diffusion of soluble intermediate polysulphides out of the cathode and accommodates volume expansion of coated sulphur particles during cycling.[18] Here, a PEG containing surfactant viz. triton-X-100 (TX-100) is tethered on to the sulphur particles (c/f ESI: Materials and Methods). The hydrophobic part of triton-X-100 (TX-100) is expected to get attached to the hydrophobic sulphur nanoparticles (SNP) with the hydrophilic part of the PEG chain projecting outwards (Fig. 1a). The tethered PEG chains are expected to coordinate lithium ions through their ether oxygen atoms (-O-CH_2-CH_2-O-) and transport the ionsthrough the polyether chains forming an extended Li^+ ion conducting network around the SNP. We envisage that this approach is superior to merely embedding SNP in an external ion conducting polymer matrix. Tethering of polymer chains on SNP will lead to result in efficient fast ion conducting pathways and prevent phase segregation between the polymer and SNP. This SNP-TX system after being lithiated (SNP-TX-Li) is wrapped up with the electronically conducting (p-doped) PAni (c/f ESI: Materials and Methods) thus, forming effectively a mixed ionic-electronic conducting SNP-TX-Li system (abbreviated as S-MIEC). In the following sections we discuss the findings obtained from various spectroscopic characterizations and electron microscopy. We also demonstrate the ability of the S-MIEC to conduct both ions and electrons and their utility as cathode in Li-S battery.

Thermogravimetric analysis (TGA) of S-MIEC is shown in Fig S1. The amount of sulphur present in S-MIEC was evaluated as 75 % from first weight loss at 168° C in TGA data and used to calculate specific capacity of battery.

The powder X-ray diffraction (PXRD) (Fig. 1b) shows that SNP in S-MIEC is in the Fdd orthorhombic structure (JCPDS no: 01-078-1889). No extra peaks in SNP-TX other than sulphur (Figures 1b and S2a) are observed suggesting absence of any

other phase or reactant material. The broad humps around 2Θ = 10°-20° in the XRD pattern of S-MIEC which is not present in SNP-TX and sulphur (Fig. 1b and S2) are attributed to the presence of PAni.[19]

Infrared spectroscopy is employed extensively to characterize the presence of various components at various stages of synthesis of S-MIEC. The exact mode of binding of TX-100 on the surface of sulphur nanoparticle is initially determined (Fig. S3) followed by the exact mode of Li^+ binding in S-MIEC. In order to determine this, TX-100 is first lithiated by dissolving LiTFSI in it to make a 1 M solution and infrared spectra of the solution is compared to that of SNP-TX-Li (Fig. 1c).

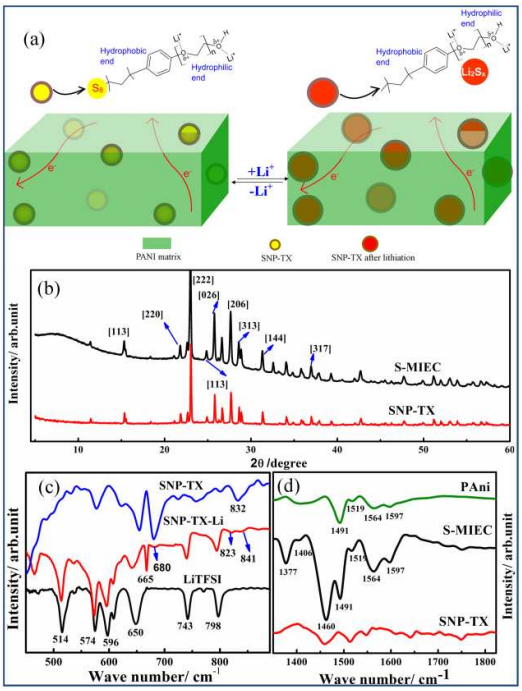

Fig. 1.(a) Schematic representation (before and after lithiation) and (b) PXRD of S-MIEC (c) and (d) FTIR spectra of various materials including s-MIEC.

The surfactant TX-100 (Fig. 1a) contains non-polar trimethylbutyl and benzenoid groups head groups attached to a polar tail chain comprising of aromatic ether attached to aliphatic long PEG chain. The synthesized hydrophobic SNP is expected to be capped by TX-100 through the hydrophobic head group of TX-100 only. The SNP-TX shows characteristic bands that can be assigned to aliphatic (1186 cm^{-1} and 833 cm^{-1}), aromatic ether (1108 cm^{-1}, 1247 cm^{-1}, 654 cm^{-1} and 680 cm^{-1}), O-H (3435 cm^{-1}), benzenoid (1400-1600 cm^{-1}), "umbrella" methyl (1353 cm^{-1}, 1364 cm^{-1}) and -CH_2 (2874 cm^{-1}, 2922 cm^{-1}, 2955 cm^{-1}) groups (c/f Table ST1 in ESI).[20,21]The intense band at 1108cm^{-1} and the weak band at 1186 cm^{-1} are assigned to the asymmetric stretching vibration of aromatic ether (Ar-O-C), and aliphatic ether (C-O-C group) of TX-100 respectively. No substantial shift in the band position is observed as compared to TX-100 (Fig. S3). This trend is also observed for other functional groups of the hydrophilic PEG chain of the SNP-TX viz. O-H stretching vibration (3434 cm^{-1}) and symmetric and asymmetric stretching vibration of -CH_2 (2867 cm^{-1} and 2954 cm^{-1}). The hydrophobic end of triton however, shows substantial change in SNP-TX as compared to TX-100. The twin bands at 1353 cm^{-1} and 1364 cm^{-1} of TX-100 assigned to the "umbrella" bending modes of tertiary butyl group appeared as a single broad band at 1358 cm^{-1} in SNP-TX (c/f Fig. S3). The intense band at 1465 cm^{-1} in TX-100 assigned to the aromatic C-C stretch appears at 1459 cm^{-1} in SNP-TX. From these observations it is speculated that TX-100 indeed binds to SNP only through its hydrophobic end. The lithiation in SNP-TX (SNP-TX-Li) is also ascertained from IR spectroscopy. In Fig. 1b), the bands at 680 cm^{-1} and 832 cm^{-1} inSNP-TX, which are respectively assigned to the phenolic ether stretch and ν_{asym}(C-O-C) of aliphatic ether are observed to broaden in SNP-TX-Li. Further, the band at 832 cm^{-1} split into two weak bands at 823 cm^{-1} and 841 cm^{-1} upon lithiation. The splitting and broadening of ether bands indicate weak interaction of lithium-ion with ether groups. Moreover SNP-TX-Li shows an extra band at 665 cm^{-1} which can be attributed to Li-O bond[22] formed by Li^+-ion binding to PEG chain in SNP-TX.

The binding of Li^+-ion is further confirmed by comparing the infrared spectrum of SNP-TX-Li with solid LiTFSI salt (Fig. S4). The $\nu_{asym}(SO_2)$ twin bands at 1322 cm^{-1} and 1336 cm^{-1} in unbound LITFSI disappears in SNP-TX-Li giving way to a new intense band appearing at 1329 cm^{-1}. Similar observation is also observed for the asymmetric stretching vibrations of S-N-S group of LiTFSI. Instead of the twin bands at 1056 cm^{-1} and 1068 cm^{-1} in the unbound LiTFSI, a single broad band is observed at 1058 cm^{-1} in SNP-TX-Li. These observations suggest that the binding of LiTFSI to the PEG chain in SNP-TX is possibly through the O-Li^+ interaction. The interaction O-Li^+ is clearly visible in the IR spectra of TX-100-LiTFSI (Fig. S5). The aromatic ether band at 1108 cm^{-1} in TX-100 split into three bands at 1164 cm^{-1}, 1109 cm^{-1} and 1135 cm^{-1} in TX-100-LiTFSI. Similarly, a new band appears at 1229 cm^{-1} along with band at 1247 cm^{-1} in TX-100-LiTFSI instead of the single aromatic ether band at 1247 cm^{-1} in TX-100. On the other hand, the aliphatic ether band at 1186 cm^{-1} is also shifted to higher wavelength at 1198 cm^{-1} in TX-100-LiTFSI. The broadening and shifting of ether bands of TX-100 after lithiation confirm interaction of lithium-ion to ether group of pure TX-100 and also in TX-100 tethered on sulphur nanoparticles. Moreover the presence of ν(C-C) of benzenoid (at 1447 cm^{-1}, 1487 cm^{-1} and 1508 cm^{-1}) and ν(-CH_2) group (2867 cm^{-1}, 2923 cm^{-1} and 2952 cm^{-1}) further supports the Li^+ binding to the ether groups. In the S-MIEC presence of conducting form of (acid-doped) PAni is very much essential for sustaining electron transport. The presence of characteristic bands like ν(C-N) (1406 cm^{-1}) and ν(C-C) of benzenoid group (1491 cm^{-1} and 1564 cm^{-1}), signature quinoid band (1519 cm^{-1}), ν(protonated imine) (1597 cm^{-1})[23]signifies presence of protonated PAni in S-MIEC.

The binding of Li^+ in SNP-TX-Li (the ion transport channel) and subsequently wrapped up with PAni is further confirmed from X-ray photo electron spectroscopy (XPS) (Fig. 2a). The XPS O1s spectrum of SNP-TX (Fig. S6) is deconvoluted into two peaks at 531.3 eV and 532.5 eV, which are characteristics of aliphatic C-O-C and/or C-OH functional group and phenolic ether

group[24]of TX-100 respectively. The O 1s spectrum of SNP-TX-Li (Fig.2a) however, is deconvoluted into four peaks. The position of the aliphatic and phenolic ether groups remained the same at 531.6 eV and 532.6 eV respectively. However, the two additional peaks at higher binding energies (533 eV and 533.7 eV) can be assigned to Li^+ bound aliphatic and phenolic ether groups respectively. Thus, the lithiated SNP-TX-Li contains both free as well as the Li^+ bound ether groups (i.e. lithium binds to both types of ether groups). Much higher intensity of Li^+ bound aliphatic ether (533.0 eV) as compared to that of phenolic ether group (533.7 eV) reflects higher extent of lithium binding in the former compared to the latter. Hence, lithium in SNP-TX-Li binds to the ether (PEG) chains of the TX-100, preferably binding to the aliphatic ether group. No changes are found in the C1s spectrum of SNP-TX upon lithiation.

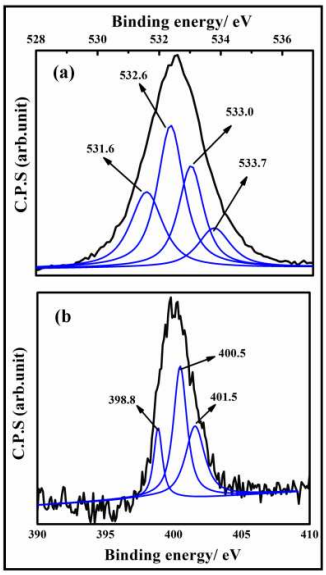

Fig. 2 (a) X-ray photo electron spectra (O1s) of SNP-TX-Li and (b) N1s spectra of S-MIEC.

The XPS N 1s spectrum of S-MIEC (Fig. 2b) can be deconvoluted into three peaks and are assigned to the benzenoid amine group (398.8 eV) and positively charged nitrogen atoms of the quinoid ring (400.5 eV and 401.5 eV) respectively. These are the characteristic bands for protonated PAni.[25]This indicates the presence of conductive (emaraldine salt) form of PAni in S-MIEC. Thus the IR and XPS results strongly suggest simultaneous presence of both the ion conducting pathways constituted by lithiated PEG chains and electronic conducting network formed by PAni.

Scanning electron microscopy (SEM) images of S-MIEC are shown in Fig. 3a. The patches seen in the SEM image clearly indicate the presence of PAni in S-MIEC. The presence of small particles of sulphur are evident from the SEM elemental mapping (Fig. 3b-e). The elemental mapping with reference to sulphur, carbon and nitrogen also show a uniform distribution of these elements in the S-MIEC matrix. Additional information about the morphology of S-MIEC and shapes of SNP in S-MIEC is obtained from the high resolution transmission electron microscopy (HRTEM) images (Fig. 4). The atomic lattice fringes (Fig. 4a) clearly indicate the highly crystalline nature of SNPs in S-MIEC. The average particle size obtained from sampling over several hundred SNPs is equal to ≈5 (± 2) nm for the SNPs. As far as our knowledge this is the very first report which discusses usage of such ultra-small nanocrystals of sulphur in this specific configuration for prospective use in batteries. (The average crystal size for S-MIEC using Scherrer formula is 45 nm. However, as is well known for small particle sizes, < 100 nm, size estimated using this formula are usually not reliable and one has to rely heavily on electron microscopy especially transmission electron microscopy for estimation of particle sizes)

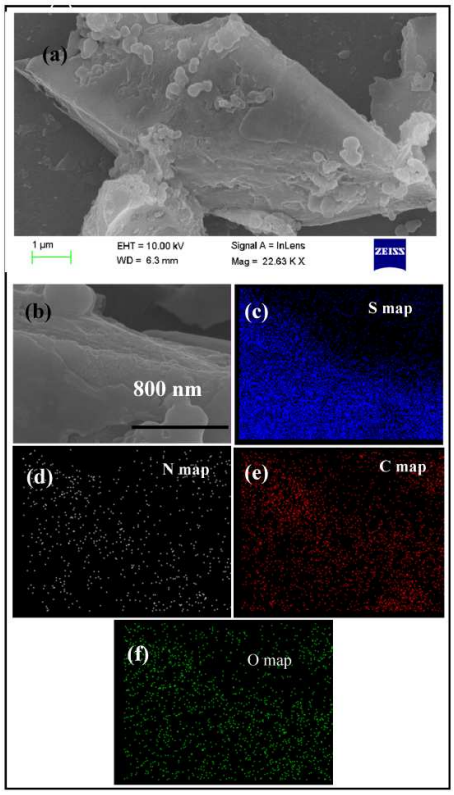

Fig. 3 (a) SEM micrographs of S-MIEC. EDX elemental mapping of S-MIEC with reference to sulphur (c), nitrogen (d), carbon (e) oxygen (f) based on the area shown in (b)

An HRTEM image of a single SNP nanocrystals (Fig. 4b) shows the lattice fringes spacing of 0.38 nm that corresponds to the (222) of Fdd orthorhombic structure of sulphur (JCPDS No. 01-078-1889). This is further crosschecked from the fast Fourier size transform (FFT) pattern (Fig. 4b Inset) generated from the HRTEM image and a d-spacing of 0.37 nm is obtained. The selected area electron diffraction (SAED) pattern of S-MIEC (Fig. 4c) further provides evidence for the nanocrystalline nature of SNPs in the S-MIEC. The SAED patterns are indexed to reflections like (206), (113), (315), (359) and (222) of Fdd orthorhombic sulphur. These reflections match well with the PXRD pattern of S-MIEC (Fig. 1b) and sulphur (Fig. S2).

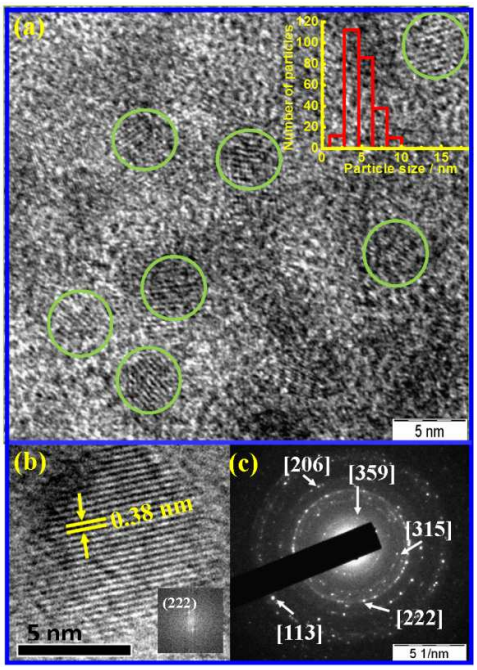

Fig. 4 (a) High resolution transmission electron microscopy (HRTEM) images of S-MIEC (inset: particle size distribution), (b) HRTEM image of a single particle showing lattice fringes (inset: FFT pattern) and (c) SAED pattern of S-MIEC.

Mixed conductivity of the S-MIEC is ascertained from the dc current-voltage (I-V) and ac-impedance spectroscopy (Fig. 5) measurements performed on a pellet of S-MIEC. The S-MIEC pellet is sandwiched in a homemade impedance cell. Two probe I-V measurements are performed over a voltage range of -5 V to +10 V and nonlinear behaviour is shown in Fig. 5a. I-V measurement of pristine acid doped PAni is performed as a reference (inset in Fig. 5a). The S-MIEC shows a nonlinear I-V response very similar to that of PAni (acid-doped). The electrical conductivity was evaluated from the I-V graph by using

$$\sigma_e = \frac{l}{AR}$$ [26]

(where l is the distance between two electrodes, A the area of electrodes and R the resistance). R in S-MIEC is obtained by extrapolating the tangent on voltage axis. The electrical conductivity obtained from the dc measurement is (1.04 ± 1.1) $\times 10^{-5}$ $\Omega^{-1}cm^{-1}$ for S-MIEC. A slightly lower estimated conductivity of S-MIEC compared to pristine PAni (4.3×10^{-5} $\Omega^{-1}cm^{-1}$, Fig. 5a inset) is not at all surprising. The lower electronic conductivity can be attributed to the presence of insulating sulphur (electrical conductivity = 2.0×10^{-17} $\Omega^{-1}cm^{-1}$ at 25°C) capped with electrically non-conducting TX-100 which is wrapped up with the conducting PAni matrix. However, this value of electrical conductivity of S-MIEC is expected to be sufficient for sustaining an efficient electrochemical process and is much higher than that reported other system e.g. mixed conducting $LiFePO_4$/ P3HT-PEO system relevant for lithium ion battery.[15a]The room temperature Nyquist plot of S-MIEC (Fig. 5b) exhibits two distinct semicircles one in the 10 KHz - 1 MHz frequency ranges and other at the low frequency ranges (1 Hz - 10 KHz). The spectra are fitted using the Maxwell equivalent circuit proposed in ref. 27 and ref 15a for analysing mixed conductivity data (inset of Fig. 5b).Here R1 and R2 are the resistances from electronic and ionic contributions to the total conductivity (CPE1and CPE2 are constant phase elements related to geometric capacity and double layer capacitance of electrode/polymer interface respectively). The ionic conductivity was evaluated to be $4.5\times10^{-6}\Omega^{-1}cm^{-1}$. Electrical contribution (σ_e) of S-MIEC is estimated to be 3.3×10^{-5} $\Omega^{-1}cm^{-1}$ and this value is very close to that obtained from dc measurement ($(1.04\pm1.1)\times10^{-5}$ $\Omega^{-1}cm^{-1}$). The impedance spectrum of SNP-TX-PAni before lithiation (inset of the Fig. 5b) exhibits only one semicircle characteristic of single-type electrical conductor. The electrical conductivity obtained from impedance measurement (inset of Fig. 5b) for the non-lithiated sample equals 2.1×10^{-5} $\Omega^{-1}cm^{-1}$ which is again very similar to that obtained for the lithiated sample (3.3×10^{-5} $\Omega^{-1}cm^{-1}$). This clearly signifies that the electrical conductivity is not altered significantly due to the presence of ion-conducting channels around the SNP. The higher value (one order) of electronic contribution to total conductivity compared to ionic contribution may be due to the fact that conducting PEG chain is not only tethered on ionically insulating sulphur nanoparticle but also wrapped up with the ionically insulating PAni matrix. The presence of ionically insulating sulphur nanoparticle and PAni around PEG chain may result in lower ionic contribution compared to the electrical one. Further, ion conducting pathways formed through short length PEG chains (each TX-100 contains 7.5 numbers of PEG chain) unlike longer chain length in ionic conducting PEO based polymer electrolytes.[28]Less extended ionic pathways on SNP surface can also be a reason of slightly lower ionic conductivity of S-MIEC compared to many ion conducting polymer electrolytes. Indeed, the ionic conductivity achieved with the electrode is comparable to solid ion conductors.

The cyclic voltammograms of S-MIEC (Fig. 6a) clearly shows the distinct voltage peaks related to charge and discharge processes. Two well defined discharge peaks are observed at 2.3 V and 1.9 V in the cathodic cycle. The first peak at 2.3 V is assigned to the reduction of S_8 to S_8^{2-} and the one at 1.9 V is the signature of reduction of higher (Li_2S_n, $4 \le n \le 8$) to lower order polysulphides (Li_2S_n, $2 \le n \le 4$).[29]The oxidation peak at 2.5 V is attributed to oxidation of Li_2S_2 and Li_2S into soluble polysulphides. No substantial shift in both cathodic and anodic peaks are observed in the subsequent cycles (Fig. 6a) as compared to the SNP-TX-PAni (before lithiation) signifying superior cycling stability of the former (Fig.S8).The speculation that charge transport in S-MIEC will be efficient and faster within the material itself and at the electrode-electrolyte surfaces is additionally reflected in the cyclic voltammetry result. The improvement in current response in S-MIEC compared to SNP-TX-PAni may be attributed to the enhancement in ionic conductivity as a result of the presence of lithium ion conducting channels upon lithiation of SNP-TX-PAni (S-MIEC).A weak peak at around 2.00 V is observed in

thecathodic cycle of SNP-TX-PAni, which shows slightly shifts in the subsequent cycles (Fig.S8).

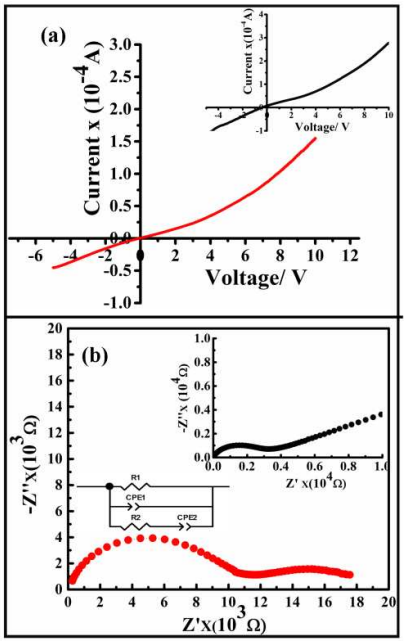

Fig. 5 (a) I-V plot for S-MIEC (inset: I-V plot of doped PAni) and (b) Nyquist plot for S-MIEC from the impedance measurement (Inset: Nyquist plot of SNP-TX-PAni). The equivalent circuit for fitting the impedance data is also shown as the inset.

This peak is attributed to stepwise reduction of higher order polysulphides. Absence of this peak in S-MIEC suggests suppression of polysulfide shuttle mechanism to a reasonable extent. The presence of excess lithium ions in S-MIEC around SNP (because of the tethered lithiated PEG chains) may help the diffusing out polysulphides to react with the Li^+ ions and arrest their movement out of cathode. Further, the presence of lithiated PEG chains may avoid the loss of Li^+ions during charging of the cell. The non-lithiated PEG chains (ether groups) may capture the exiting Li^+ ($8Li_2S \rightarrow 16Li+ S_8$) while charging the cell (delithiation), resulting in decrease in reversibility and Coulombic efficiency. This is also observed in the GITT result which exhibits a lithiation process of 1.9 Li in S-MIEC as compared to only 1.01 Li in SNP-TX-PAni.

The galvanostatic cycling performance of S-MIEC is shown in Fig. 6band 6c along with that of SNP-TX-PAni. The specific capacity of S-MIEC at the 1st discharge cycle is 1669 $mAhg^{-1}$, which is very close to the theoretical capacity of sulphur (≈ 1675 $mAhg^{-1}$). The SNP-TX-PAni shows a capacity of 1055 $mAhg^{-1}$ in the first cycle. On charging, the first cycle capacity of S-MIEC and SNP-TX-PAni are observed to be 1670 $mAhg^{-1}$ and 1057 $mAhg^{-1}$respectively. In spite of the initial decrease in capacity from 1669 $mAhg^{-1}$ (1^{st}) to 1012 $mAhg^{-1}$(2^{nd}) cycle, the capacity values very rapidly stabilized within 30 to 100 cycles and recorded a stable value of 900 mAh g^{-1} from 60-100 cycles. The retention of capacity in S-MIEC is 88%. The non-lithiated sample however, shows only 34% retention in capacity (2^{nd} cycle capacity: 951 $mAhg^{-1}$ and 100^{th} cycle capacity 320 $mAhg^{-1}$). Thus, upon lithiation S-MIEC shows better cycling stability compared to the SNP-TX-PAni. Moreover, the observed cycling performances of S-MIEC was superior compared to recently reported conducting polymer based sulphur composite electrodes.[30]The Coulombic efficiencies (Fig. 6b inset) for both the samples were similar, nearly 100% in the initial cycles. However, at the end of the 100^{th} cycle Coulombic efficiency decreased to 71% for SNP-TX-PAni whereas S-MIEC retained a Coulombic efficiency of 98%.

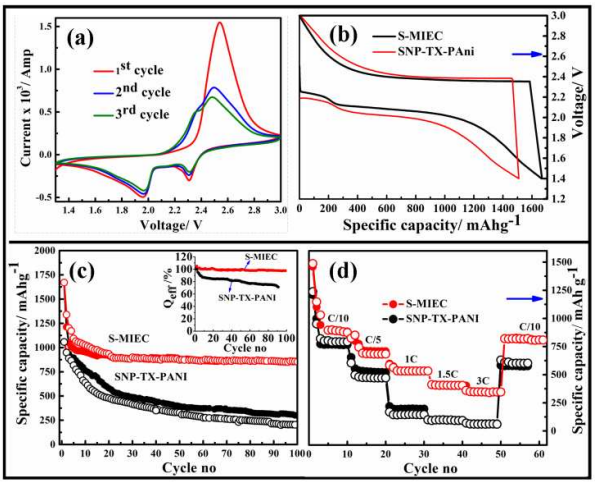

Fig. 6 (a) Cyclic voltammograms (scan rate = 0.25 mV S^{-1}), (b) voltage versus specific capacity plot (xLi represents the extent of lithiation in Li_xS), (c) galvanostatic cycle performance efficiency (@ 0.1 C current rate) (inset: Coulombic efficiency) and (d) rate capability at various current rates from 0.1 C to 3C of S-MIEC.

The rate capability of the S-MIEC and SNP-TX-PAni cathodes are cycled at various current rates from 0.1 C to 3 C (Fig 6d). At all current rates specific capacities of S-MIEC are observed to be higher than that of non lithiated counterpart. The decrease in specific capacity of lithiated sample (S-MIEC) as a function of current rates is much less as compared to the non-lithiated one. At 3 C current rate, S-MIEC shows a capacity of 346 mAh g^{-1}, more than five times higher than SNP-TX-PAni (≈ 64 mAh g^{-1}). Thus, rate capability is enormously improved following the building up of lithium conducting channel. This is understood on the basis that at higher current rates ions cannot move as fast as electron through the interfaces and resulting in decrease in specific capacity. However, in S-MIEC the lithium ion can move fast. Improved cycle performance in S-MIEC compared to SNP-TX-PAni is also reflected in the number of Li^+ ion (x_{Li+}) involved in the reaction S+ xLi→Li_xS. For S-MIEC, x_{Li}= 1.9 (Fig. 7a)compared to x_{Li}= 1.01 in SNP-TX-PAnisignifies better charge transfer in the former compared to the latter.

Electrode kinetics for S-MIEC cathode is investigated by galvanostatic intermittent titration technique (GITT) (Fig. 7a). The basic mechanism for ion transport through electrodes (rate determining step for electrochemical reaction at electrode surfaces) is the translational diffusion guided by the concentration gradient. Faster chemical diffusion leads to faster ionic mobility and facile transport, thus improving

reversible charge-discharge reaction and better cycle life. The Li^+ chemical diffusion coefficient (D_{Li}) for S-MIEC is calculated from the GITT polarization curve (c/f Fig. 7b) and by considering that the ion diffusion obeys Fick's law:[31]

$$D_{Li} = \frac{4}{\pi\tau}\left(\frac{mV_m}{MS}\right)^2\left(\frac{\Delta E_s}{\Delta E_t}\right)^2$$

(where m, M and V_m are active mass, molar mass and molar volume of sulphur respectively, and τ is the constant current pulse time; ΔE_t and ΔE_s are total change of cell voltage during current pulse and change of steady state voltage (E_0) for the particular step at the plateau potential, respectively and S the electrode surface area). The D_{Li} calculated for S-MIEC is 2.3×10^{-10} cm^2s^{-1} whereas for SNP-TX-PAni a value of 2.88×10^{-13} cm^2s^{-1} is obtained. Higher value of diffusion coefficient in S-MIEC as compared to SNP-TX-PAni indicates faster ion-diffusion via the in-built lithiatedPEG chains to sulphur electrode and this enhances the charge transport leading to improved specific capacity and rate capability of S-MIEC compared to SNP-TX-PAni.

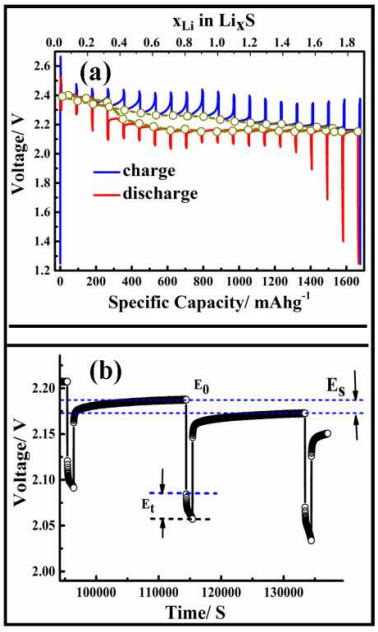

Fig. 7 (a) Galvanostatic intermittent titration technique (GITT) charge-discharge curve and (b) polarization curve for single GITT discharge- charge process at plateau potential for S-MIEC.

Superior battery performance and faster electrode kinetics for S-MIEC is further justified by electrochemical impedance spectroscopy (EIS) (Fig.S9) by measuring the impedance data before cycling and after tengalvanostatic cycles (@0.1C). Before cycling only one semicircle at medium-high frequency region is observed for the S-MIEC as compared to two semicircles at lower frequency region in SNP-TX-PAni. Resistances for S-MIEC and SNP-TX-PAni corresponding to the semicircle at lower frequency region is due to charge transfer (R_{ct}) at the electrode/electrolyte interface whereas for SNP-TX-PAni one additional depressed semicircle at lower frequency region corresponds to polymer/electrode interface. Before cycling, the R_{ct}, obtained for S-MIEC (48 Ω) and SNP-TX-PAni (57 Ω) are almost comparable. However, after the 10^{th} cycle R_{ct} for SNP-TX-PAni increase to 92 Ω (38% of before cycling data), whereas R_{ct} for S-MIEC instead decrease to 15 Ω. This implies that the interface for S-MIEC becomes more conducting during cycling compared to SNP-TX-PAni which is attributed to faster ion and electron transport at the interfaces. No significant change in bulk resistance (resistance at high frequency region before the onset of the semicircle) for both S-MIEC and SNP-TX-PAni may indicate lesser probability of polysulfide dissolution after polymer coating of SNP. The EIS result further supports enhancement in electrochemical performances of S-MIEC compared to SNP-TX-PAni due to faster ion and electron transport in S-MIEC.

3. Conclusion

In summary, we have convincingly demonstrated for the first time a unique method to retainsulphur and polysulphides within a flexible organic mixed conducting network. Configuration of ultra-small sulphur nanoparticles in a flexible and mixed conducting polymer network is shown to be superior on several counts compared to earlier approaches involving porous carbon hosts. The approach demonstrated here provides higher amounts of sulphur loading located inside the mixed conducting polymer matrix. Importantly, the flexible polymer matrices provide distinctpathways for both ion and electrons. This is remarkable as earlier approaches using hollow carbon adsorbatesprovide fast conducting pathways only to electrons. Combination of all these factors in S-MIEC contributes towards high stability and enhanced in Li-S battery performance. Additionally, the usage of S-MIEC is expectedly going to drastically reduce battery costs due to higher yields and employment of abundant and cost effective components. The concept discussed here will be extremely beneficial across various battery chemistries especially where the active storage material is an electron and ion insulator and also demonstrates extensive volume changes during the electrochemical reaction.

Acknowledgements

We thank the Centre for Nanoscience and Engineering (CENSE), Solid State and Structural Chemistry Unit (I.S. Jarali), Department of Organic Chemistry and The Society for Innovation and Development (SID), Indian Institute of Science (IISc) for providing with various instrumentation facilities. We thank the DST-Nano Mission,Govt. of India, India-Taiwan Programme of Cooperation in Science and Technology, for financial support

References

1 J. B. Goodenough, K. S. Park, *J. Am. Chem. Soc.*, 2013, **135**, 1167–1176.

2 a) J. M. Tarascon, M. Armand, *Nature*, 2001, 414, 359-367.b) B. Scrosati, J. Hassoun and Y. K. Sun, *Energy Environ. Sci.*, 2011, 4, 3287.c) G. Zhou, L. C. Yin, D. W. Wang, L. Li, S. Pei, I. R. Gentle, F. Li, H. M. Cheng, *ACS Nano*, 2013,**7**, 5367-5375. d) J. Zhang, Z. Dong, X. Wang, X. Zhao, J. Tu, Q. Su, G. Du, *J. Power Sources*, 2014, **270**, 1-8.
3 a) C. Sirisopanaporn, C. Masquelier, P. G. Bruce, A. R. Armstrong, R. Dominko, *J. Am. Chem. Soc.*,2011, **133**, 1263–1265. b) L. Croguennec, M. R. Palacin, *J. Am. Chem. Soc.*,2015, **137**, 3140–3156.
4 a) S. Brutti, V. Gentili, H. Menard, B. Scrosati, P. G. Bruce, *Adv. Energy Mater.*, 2012, **2**, 322–327. b) H. Kim, J. Cho, *NanoLett*. 2008, **8**, 3688-3691.
5 a) J. Kim, D. J. Lee, H. G. Jung, S. M. Lee, Y. K. Sun, J. Hassoun, B. Scrosati, *Adv. Funct. Mater.*, 2013, **23**, 1076–1080. b) Z. Lin, Z. Liu, W. Fu, N. J. Dudney, C. Liang, *Angew. Chem. Int. Ed.*, 2013, **52**, 7460 –7463.
6 a) J. Guo, Z. Yang, Y. Yu, H. D. Abruña, L. A. Archer, *J. Am. Chem. Soc.*,2013, **135**, 763–767. b)M. Barghamadi, A. S. Best, A. I. Bhatt, A. F. Hollenkamp, M. Musameh, R. J. Rees, T. R¨uther,*Energy Environ. Sci.*, 2014, **7**, 3902–3920.
7 M. Vizintin, U. M Patel, B. Genorio, R. Dominko, *ChemElectroChem*, 2014, **1**, 1040–1045.
8 A. Manthiram, A. Fu, S. H. Chung, Zu, Y. S. Su, *Chem. Rev.*, 2014, **114**, 11751–117877.
9 S. Evers, L. F. Nazar,*Acc. Chem. Res.*, 2013, **46**, 1135– 1143.
10 U. M. Patel, R. Dominko, *ChemSusChem*, 2014, **7**, 2167–2175.
11 a) Z. Yang, J. Guo, S. K. Das, Y.Yu, Z. Zhou, H. B. Bru˜nab, L. A. Archer, *J. Mater. Chem. A*, 2013, **1**, 1433–1440.b) G. C. Li, G. R. Li, S. H. Ye, X. P. Gao, *Adv. Energy Mater.*, 2012, **2**, 1238–1245.
12 N. Jayaprakash, J. Shen, S. S. Moganty, A. Corona, L. A. Archer, *Angew. Chem. Int. Ed.*, 2011, **50**, 5904 –5908.
13 M. Cuisinier, P. E. Cabelguen, B. D. Adams, A. Garsuch, M. Balasubramanianc, L. F. Nazar, *Energy Environ. Sci.*, 2014, **7**, 2697–2705.
14 Z.Yuan, H. J. Peng, J. Q. Huang, X. Liu, D. W. Wang, X. B. Cheng, *Adv. Funct. Mater.*, 2014, **24**, 6105–6112.
15 a) A. E. Javier, S. N. Patel, D. T. Hallinan, V. Srinivasan, N. P. Balsara, *Angew. Chem. Int. Ed.*, 2011, **50**, 9848-9851. b) Y. Fu, A. Manthiram, *Chem. Mater.*, 2012, **24**, 3081-3087. c) B. H. Jeon, J. H. Yeon, K. M. Kim, I. J. Chung,*J. Power Sources*, 2002, **109**, 89-97.
16 a) J. L.Bredas, G. B. Street, *Acc. Chem. Res.*, 1985, **18**, 309-315. b) C. R. Menon, C. O. Yoon , D. Moses , A. J. Heeger, *Handbook of Conducting Polymers* (Eds.: T. A. Skotheim, R. L. Elsenbaumer, J. R. Reynolds), 2nd ed. Marcel Dekker, New York, 1998. c) F. Yakuphanoglu, B. F. Senkal, *J. phys. Chem. C*, 2007, **111**, 1840-1846. d) J. Stejskal, I. Sapurina, M. Trchova, J. Prokes, E. Tobolkova, *Macromolecules*, 1998, **31**, 2218-2222. e) A. B. Kaiser, *Rep. Prog. Phys.*, 2001, **64**, 1-49.
17 H. Gao, Q. Lu, N. Liu, X. Wang, F. Wanga, *J. Mater. Chem. A*, 2015, **3**, 7215–7218.
18 H. Wang, Y. Yang, Y. Liang, J. T. Robinson, Y. Li, A. Jackson, Y. Cui, H. Dai, *Nano Lett.*, 2011, 11, 2644-264.
19 L. Yang, J. Zhu, D. Xiao, *RSC. Adv.*, 2012, **2**, 8179-8188.
20 B. C. Smith, *Infrared Spectral Interpretation: A systematic approach*, CRC press, USA, 1998, p 79.
21 Daimay. Lin- Vien, Norman B. Colthup, williumG.Fateley, Jeanette G. Grasselli, *The Hand Book of Infrared and Raman Characteristic Frequencies of Organic Molecules*, Academic Press, United kingdom, 1991.
22 a) L. Rey, P. Johansson, J. Lindgren, J. C. Lassegues, J. Grondin, L. Servant, *J. Phys. Chem. A*, 1998, **102**, 3249-3258. b) N. Bar, P. Basak, *J. Phys. Chem. C*, 2014, **118**, 10640−10650.
23 G. S. Kim, Y. J. Lim, H. J. Sung, J. H. Choi, Y. Seo, *Polymer*, 2007, **48**, 6622-6631.
24 a) G. P. Lopez, D. G. Castner, B. D. Ratner, *Surface and Interface Analysis*, 1991, **17**, 267-272. b) A. D. Bendrea, G. Fabregat, L. Cianga, F. Estrany, L. J. Valle, I. Cianga, C. Alem´an, *Polym. Chem.*, 2013, 4, 2709–2723.
25 a) M. Aldissi, S. P. Armes, *Macromolecules*, 1992, **25**, 2963-2968. b) L. Zhang, H. Peng, D. Zoran, Z. Paul, A. Kilmartin, J. T. Sejdic, *Macromol.Chem. Phys.*, 2007, **208**, 1210–1217.
26 H. A. Bioki, M. B. Zarandi, *Indian J. Phys.*, 2012, **86**, 439-441.
27 J. PlÇocharski, H. Wycis´lik, *Solid State Ionics*, 2000, **127**, 337-344.
28 a) H. Z. Stoeva, I. Martin-Litas, E. Staunton, Y. G. Andreev, P. G. Bruce, *J. Am. Chem. Soc.*, 2003, **125**, 4619-4626. b) C. Zhang, S. Gamble, D. Ainsworth, A. M. Slawin, Y. G. Andreev, P. G. Bruce, *Nat.Mater.*, 2009, **8**, 580-584.
29 Y. J. Choia, Y. D. Chung, C. Y. Baeka, K. W. Kima, H. J. Ahna, *J. Power Sources,* 2008, **184**, 548–552.
30 a) Z. Dong, J. Zhang, X. Zhao, J. Tu, Q. Su, G. Du, *RSC Adv.,* 2013, **3**, 24914-24917. b) L. Xiao, Y. Cao, J. Xiao, B. Schwenzer, M. H. Engelhard, L. V. Saraf, Z. Nie, G. J. Exarhos, J. Liu, *Adv. Matter.,*2012, **24**, 1176-1181. c) Y. Liu, J. Zhang, X. Liu, J. Guo, L. Pan, H. Wang, Q. Su, G. Du, *Mater. Lett.,*2012, **24**, 1176-1181.
31 Y. Zhu, Y. Xu, Y. Liu, C. Luo, W. Wang, *Nanoscale*, 2013, **5**, 780–787.

Table of Content(TOC):

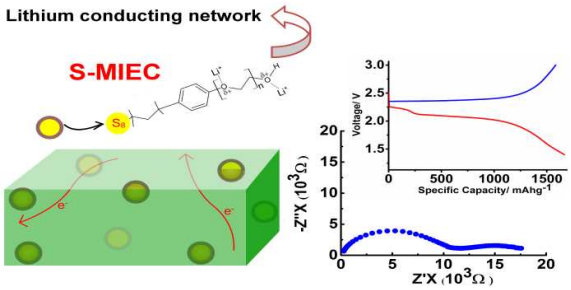

Mixed conducting S-MIEC,comprising of lithium conductingsurfactant tethered on sulphur nanoparticles andwrapped up by an electron conducting polymer,displays high degree of reversibility and fast charge transfer kinetics in a Li-S battery.